Anal. Chem. **2002,** *74,* 4763−4773

Probing Antigen−Antibody Binding Processes by Impedance Measurements on Ion-Sensitive Field-Effect Transistor Devices and Complementary Surface Plasmon Resonance Analyses: Development of Cholera Toxin Sensors

Maya Zayats, Oleg A. Raitman, Vladimir I. Chegel,† Andrei B. Kharitonov, and Itamar Willner*

Institute of Chemistry, The Hebrew University of Jerusalem, Jerusalem 91904, Israel

Impedance measurements on ISFET devices are employed to develop new immunosensors. The analysis of the transconductance curves recorded at variable frequencies, upon the formation of antigen−antibody complexes on the ISFET devices, allows determination of the biomaterial film thicknesses. Complementary surface plasmon resonance measurements of analogous biosensor systems, using Au-coated glass slides as support, reveal similar film thicknesses of the biomaterials and comparable detection limits. A dinitrophenyl antigen layer is immobilized on the ISFET gate as a sensing interface for the anti-dinitrophenyl antibody (anti-DNP-Ab). The anti-DNP-Ab is analyzed with a sensitivity that corresponds to 0.1 μg mL^{-1}. The assembly of the biotinylated anti-anti-DNP-Ab and avidin layers on the base anti-DNP-Ab layer is characterized by impedance measurements. The development of an ISFET-based sensor for the cholera toxin is described. The anti-cholera toxin antibody is immobilized on the ISFET device. The association of the cholera toxin (CT) to the antibody is monitored by the impedance measurements. The detection limit for analyzing CT is 1.0 $\times$ 10^{-11} M.

The optical and electronic transduction of the formation of antigen−antibody complexes on surfaces is of fundamental interest for the development of biosensors.[1] Reflectometric interference spectroscopy and surface plasmon resonance[2,3] (SPR) represent two sensitive optical means for the detection of antigen−antibody binding processes on surfaces. Electronic transduction of antigen−antibody interactions on surfaces was accomplished by electrochemical or acoustic wave methods. Amperometric detection of immunological recognition events was accomplished by the use of enzyme−antibody conjugates that generate electroactive products,[4] by the use of redox-labeled antigens or antibodies for competitive assay,[5] or by the use of redox-labeled enzymes[6] or electroactive components[7] as electrochemical probes. Electrochemical analysis of antigen−antibody binding events in "label-free" systems was accomplished by capacitance[8] or impedance measurements.[9] Microgravimetric, quartz crystal microbalance, measurements were widely employed for the detection of antigen−antibody complexes on piezoelectric crystals.[10]

Ion-sensitive field-effect transistors (ISFETs) find growing interest in the rapidly developing field of bioelectronics.[11] The control of the gate potential of the ISFET device by biocatalyzed transformations leads to enzyme-based FET devices (ENFETs).[12] Similarly, enzyme-labeled antigens or antibodies were employed as conjugates for controlling the gate potential as a result of the

* To whom correspondence should be addressed. Tel: 972-2-6585272. Fax: 972-2-6527715. E-mail: willnea@vms.huji.ac.il.

† On leave from the Institute of Physics of Semiconductors, National Academy of Sciences of Ukraine, Kiev, Ukraine.

(1) (a) Willner, I.; Katz, E. *Angew. Chem., Int. Ed.* **2000**, *39*, 1180−1218. (b) Willner, I.; Katz, E.; Willner, B. In *Sensor Updates*; Balted, H., Göpel, W., Hesse, J., Eds.; Wiley-VCH: Weinheim, Germany, 1999; Vol. 5, pp 45−102. (c) Göpel, W. *Biosens. Bioelectron.* **1995**, *10*, 35−59. (d) Willner, I.; Willner, B. *Trends Biotechnol.* **2001**, *19*, 222−230.

(2) (a) Brecht, A.; Ingenhoff, J.; Gauglitz, G. *Sens. Actuators, B* **1992**, *6*, 96−100. (b) Striebel, C.; Brecht, A.; Gauglitz, G. *Biosens. Bioelectron.* **1994**, *9*, 139−146. (c) Lang, G.; Brecht, A.; Gauglitz, G. *Fresenius' J. Anal. Chem.* **1996**, *68*, 857−860.

(3) (a) Knoll, W. *Annu. Rev. Phys. Chem.* **1998**, *49*, 569−638. (b) Badia, A.; Arnold, S.; Scheumann, V.; Zizlsperger, M.; Mack, J.; Jung, G.; Knoll, W. *Sens. Actuators, B* **1999**, *54*, 145−165. (c) Kruchinin, A. A.; Vlasov, Y. G. *Sens. Actuators, B* **1996**, *30*, 77−80.

(4) (a) Hadas, E.; Soussan, L.; Rosen-Margalit, I.; Farkash, A.; Rishpon, J. *J. Immunoassay* **1992**, *13*, 231−252. (b) Ivnitski, D.; Rishpon, J. *Biosens. Bioelectron.* **1996**, *11*, 409−417. (c) Rishpon, J.; Ivnitski, D. *Ann. N.Y. Acad. Sci.* **1996**, *799*, 508−513. (d) Stoytcheva, M. *Electroanalysis* **1995**, *7*, 660−662. (e) Wijayawardhana, C. A.; Halsall, H. B.; Heineman, R. *Anal. Chim. Acta* **1999**, *399*, 3−11.

(5) Aizawa, M. In *Electrochemical Sensors in Immunological Analysis*; Ngo, T. T., Ed.; Plenum Press: New York, 1987; pp 269−291.

(6) (a) Blonder, R.; Katz, E.; Cohen, Y.; Itzhak, N.; Riklin, A.; Willner, I. *Anal. Chem.* **1996**, *68*, 3151−3157. (b) Ho, W. O.; Athey, D.; McNeil, C. J. *Biosens. Bioelectron.* **1995**, *10*, 683−691.

(7) Katz, E.; Willner, I. *J. Electroanal. Chem.* **1996**, *418*, 67−72.

(8) (a) Bresler, H. S.; Lenkevich, M. J.; Murdock, J. F., Jr.; Newman, A. L.; Robbin, R. O. In *Biosensor Design and Application*; Mathewson, P. R., Finley, J. W., Eds.; ACS Symposium Series 511; American Chemical Society: Washington, DC, 1992; Chapter 9, pp 89−104. (b) Mirsky, V. M.; Riepel, M.; Wolfbeis, D. S. *Biosens. Bioelectron.* **1997**, *12*, 977−989. (c) Berney, H.; Alderman, J.; Lane, W.; Collins, J. K. *Sens. Actuators, B* **1999**, *57*, 238−248.

(9) (a) Patolsky, F.; Filanovsky, B.; Katz, E.; Willner, I. *J. Phys. Chem. B* **1998**, *102*, 10359−10367. (b) Alfonta, L.; Bardea, A.; Khersonsky, O.; Katz, E.; Willner, I. *Biosens. Bioelectron.* **2001**, *16*, 645−687.

(10) (a) Bardea, A.; Katz, E.; Willner, I. *Electroanalysis* **2000**, *12*, 1097−1106. (b) Blonder, R.; Ben Dov, I.; Dagan, A.; Willner, I.; Zisman, E. *Biosens. Bioelectron.* **1997**, *12*, 627−644. (c) Suleiman, A. A.; Guilbault, G. G. *Analyst* **1994**, *119*, 2279−2282. (d) Pavey, K. D.; Ali, Z.; Olliff, C. J.; Paul, F. *J. Pharm. Biomed. Anal.* **1999**, *20*, 241−245. (e) Abad, J. M.; Pariente, F.; Hernandez, L.; Lorenzo, E. *Anal. Chim. Acta* **1998**, *368*, 183−189.

10.1021/ac020312f CCC: $22.00
Published on Web 08/17/2002

formation of the antigen−antibody complexes.[13] In most of these studies, the biomaterial was encapsulated in polymeric membranes that were associated with the gate interface. In a series of studies,[14] we reported on the covalent immobilization of monolayers of biomaterials on the gate surface to form active biosensing interfaces. The monolayer configuration as sensing interface has a clear advantage since the association of the analyte lacks diffusion limitations, and thus, the detection response times of the systems is rapid.

Recently we introduced impedance spectroscopy as a method to characterize the composition and structure of protein-modified ISFET devices.[15] We have shown that impedance measurements on the ISFET devices can follow the buildup and thickness of protein layers on the gate surface, e.g., biotin−avidin or glucose oxidase layers. These measurements enabled us to estimate the surface coverage of the proteins on the gate surface. In the present study, we demonstrate that impedance measurements on the ISFET device can be used to detect antigen−antibody interactions on the gate surface. We perform complementary SPR experiments and find that the SPR and impedance measurements reveal comparable sensitivities. The two methods are applied for the development of immunosensors for the cholera toxin[16] and DNP-antibody.[17]

THEORETICAL BACKGROUND

The impedance of the membrane associated with the ISFET[15,18] can be represented by the equivalent circuit shown in Figure 1A. It consists of the input element of the ISFET device consisting of the silicon resistance, R_{Si}, the space-charge capacitance, C_{sc}, and the oxide insulator capacitance, C_{ox}, that is linked in series to the second element that corresponds to the membrane connected in series to the third element composed of the solution resistance, R_{sol}. The impedance element of the membrane is divided into two parts linked in series. One part includes the bulk membrane properties, e.g., its bulk capacitance, C_{mem}, in parallel with the membrane resistance, R_{mem}. The second part includes the interfacial properties of the membrane, composed of the double-layer capacitance, C_{dl}, in parallel to the sum of the interfacial charge-transfer resistance, R_{et}, and the Warburg impedance, W, originating from the diffusion of ions to the membrane interface. This complex circuit may be simplified in terms of the circuit depicted in Figure 1B under certain conditions. Provided that the semiconductor operates in the inversion region, C_{sc} is substantially smaller than C_{ox} and may be neglected. Similarly, the silicon resistance and solution resistance, R_{Si} and R_{sol}, respectively, are significantly smaller than the membrane resistance and thus may be neglected. The interfacial properties of the membrane make an important contribution to the circuit at low frequencies (≤5 Hz),[19] but at higher frequencies (≥5 Hz), the interfacial features of the membrane contribute little to the impedance properties of the system. This leads under the respective conditions to the simplified equivalent circuit scheme outlined in Figure 1B, where the oxide layer capacitance is in series with the element consisting of the membrane capacitance in parallel to the membrane resistance. Figure 2 shows the electronic circuit used to elucidate the impedance features of the ISFET. The voltage applied between the counter electrode and the source, V_{GS}, leads to the drain-source current, I_D. Upon the application of the small sinusoidal voltage perturbation on the counter electrode, δV_{GS}, small variations in

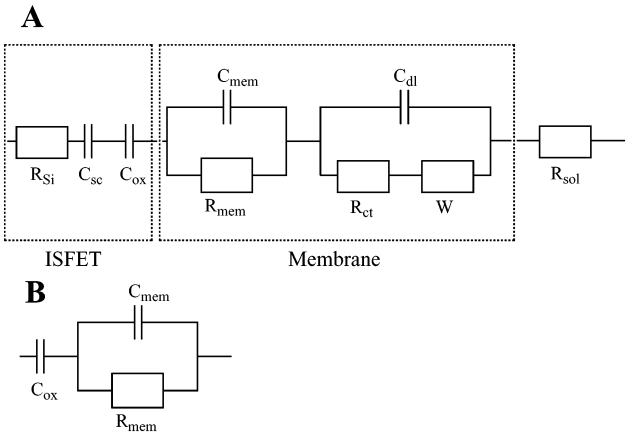

Figure 1. (A) Equivalent circuit of an ISFET device modified by a membrane film on the gate interface. (B) Simplified equivalent circuit corresponding to a membrane-functionalized ISFET device. R_{si}, R_{mem}, R_{ct}, and R_{sol} correspond to the resistances of the Si layer, the chemical sensing interface, the space charge, and solution, respectively. C_{sc}, C_{ox}, C_{mem}, and C_{dl} correspond to the space charge capacitance and the capacitance of the oxide insulating layer, of the membrane, and of the double layer, respectively. W represents the Warburg impedance.

(11) (a) Bergveld, P.; Sibbald, A. In *Comprehensive Analytical Chemistry*; Svehla, G., Ed.; Elsevier: Amsterdam, 1988; Vol. XXIII. (b) Eijkel, J. C. T.; Olthuis, W.; Bergveld, P. *Biosens. Bioelectron.* **1997**, *12*, 991−1001. (c) Ottenbacher, D.; Kindervater, R.; Gimmel, P.; Klee, B.; Jähnig, F.; Göpel, W. *Sens. Actuators, B* **1992**, *6*, 192−196. (d) Koch, S.; Woias, P.; Meixner, L. K.; Drost, S.; Wolf, H. *Biosens. Bioelectron.* **1999**,*14*, 413−421. (e) Jinghong, H.; Dafu, C.; Yating, L.; Hao, Y.; Xingxia, C.; Hong, Z. *Sens. Actuators, B* **1996**, *35*−*36*, 422−426.

(12) (a) Kharitonov, A. B.; Zayats, M.; Lichtenstein, A.; Katz, E.; Willner, I. *Sens. Actuators, B* **2000**, *70*, 222−231. (b) Volotovsky, V.; Kim, N. *Anal. Chim. Acta* **1998**, *359*, 143−148. (c) Simonian, A. L.; Grimsley, J. K.; Flounders, A. W.; Schoeniger, J. S.; Cheng, T.-C.; DeFrank, J. J.; Wild, J. R. *Anal. Chim. Acta* **2001**, *442*, 15−23. (d) Puig-Lleixá, C.; Jiménez, C.; Alonso, J.; Bartroli, J. *Anal. Chim. Acta* **1999**, *389*, 179−188. (e) Jiménez, C.; Bartroli, J.; de Rooij, N. F.; Koudelka-Hep, M. *Anal. Chim. Acta* **1997**, *351*, 169−176. (f) Soldatkin, A. P.; Volotovsky, V.; Elskaya, A. V.; Jaffrezic-Renault, N.; Martelet, C. *Anal. Chim. Acta* **2000**, *403*, 25−29.

(13) (a) Sekiguchi, T.; Nakamura, M.; Kato, M.; Nishikawa, K.; Hokari, K.; Sugiyama, T.; Asaka, M. *Sens. Actuators, B* **2000**, *67*, 265−269. (b) Collapicchioni, C.; Barbaro, A.; Porcelli, F.; Giannini, I. *Sens. Actuators, B* **1991**, *4*, 245−250. (c) Koncki, R.; Owczarek, A.; Dzwolak, W.; Glab, S. *Sens. Actuators, B* **1998**, *47*, 246−250.

(14) (a) Kharitonov, A. B.; Zayats, M.; Alfonta, L.; Katz, E.; Willner, I. *Sens. Actuators, B* **2001**, *76*, 203-210. (b) Zayats, M.; Kharitonov, A. B.; Katz, E.; Willner, I. *Analyst* **2001**, *126*, 652−657. (c) Zayats, M.; Kharitonov, A. B.; Katz, E.; Bückmann, A. F.; Willner, I. *Biosens. Bioelectron.* **2000**, *15*, 671−680.

(15) Kharitonov, A. B.; Wasserman, J.; Katz, E.; Willner, I. *J. Phys. Chem. B* **2001**, *105*, 4205−4213.

(16) (a) Terrattaz, S.; Stora, T.; Duschl, C.; Vogel, H. *Langmuir* **1993**, *9*, 1361−1369. (b) Charych, D. H.; Nagy, J. D.; Spevak, W.; Bednarsky, M. D. *Science* **1993**, *261*, 585−588. (c) Pan, J. J.; Charych, D. *Langmuir* **1997**, *13*, 1365−1367.

(17) (a) Philips, J. R.; Brouwer, W.; Edwards, M.; Mahler, S.; Ruhno, J.; Collins, A. M. *Immunol. Cell Biol.* **1999**, *77*, 121−126. (b) Willner, I.; Willner, B. *Biotechnol. Prog.* **1999**, *15*, 991−1002. (c) Mammen, M.; Gomez, F. A.; Whitesides, G. M. *Anal. Chem.* **1995**, *67*, 3526−3535.

(18) (a) Antonisse, M. M. G.; Snellink-Ruël, B. H. M.; Lugtenberg, R. J. W.; Engbersen, J. F. J.; van den Berg, A.; Reinhoudt, D. N. *Anal. Chem.* **2000**, *72*, 343−348. (b) Lugtenberg, R. J. W.; Egberink, R. J. M.; van den Berg, A.; Engbersen, J. F. J.; Reinhoudt, D. N. *J. Electroanal. Chem.* **1998**, *452*, 69−86. (c) Chovelon, J. M.; Jaffrezic-Renault, N.; Gros, Y.; Fombon, J. J.; Pedone, D. *Sens. Actuators, B* **1991**, *3*, 43−50.

(19) Armstrong, R. D.; Horvai, G. *Electrochim. Acta* **1990**, *35*, 1−7.

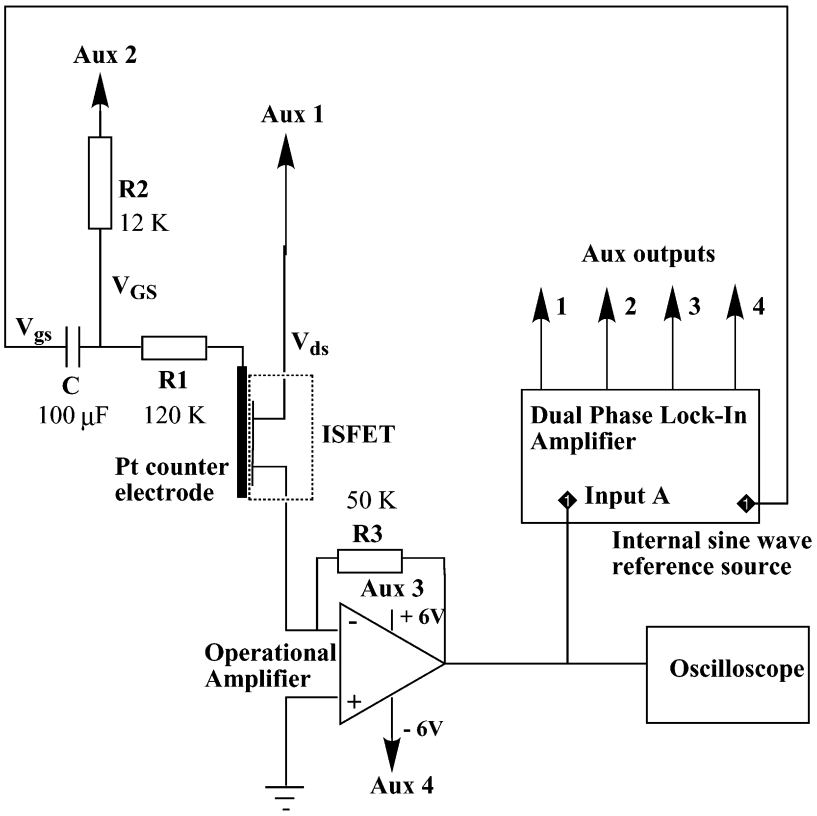

Figure 2. Electronic circuit for the determination of the transconductance of a film-modified ISFET device.

the drain current occur, δI_d. The transconductance defined as $g_m = \delta I_d/\delta V_{GS}$ is frequency-dependent.[20] When a membrane layer is associated with the oxide gate layer, the potential V_{GS} divides over the membrane and oxide layer, and thus, the effective potential difference between the gate and the source is smaller than the applied value V_{GS}. Accordingly, a frequency-dependent transfer function, $H(j\omega)$, defined by eq 1, is introduced to relate the applied

$$H(j\omega) = \frac{1 + j\omega R_{mem}C_{mem}}{1 + j\omega R_{mem}(C_{mem} + C_{ox})} \quad (1)$$

$$V_{out} = R_{gm}H(j\omega)V_{GS} \quad (2)$$

voltage to the output voltage (eq 2). This transfer function (or transconductance) basically expresses the compensation factor required to alter the output potential as a result of changes of the gate potential in order to retain the fixed drain-source current. As the chemical modification of the gate alters the impedance features of the interface, the transconductance function will include a real transconductance (controlled by the gate resistance) and an imaginary transconductance (controlled by the gate capacitance). We found, however, that the applied frequencies influence mainly the imaginary transconductance,[15] and thus, these functions are used to elucidate chemical events occurring on the gate.

The theoretical[18a,b] shape of the imaginary transconductance curve and the methods to extract the values τ_1 and τ_2 defined by eq 3 and eq 4 are shown in Figure 3. The intersection of the two

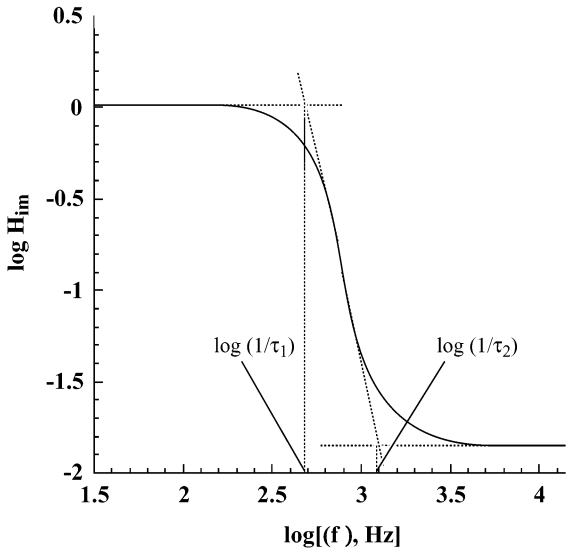

Figure 3. Theoretical transfer function and method for the extraction of the τ_1 and τ_2 values. (The transfer function H_{im} is dimensionless and is defined in eq 1).

$$\tau_1 = R_{mem}(C_{mem} + C_{ox}) \approx R_{mem}C_{ox} \quad (3)$$

$$\tau_2 = R_{mem}C_{mem} \quad (4)$$

linear segments at low frequencies yields the τ_1 value. Since at low frequencies the oxide layer capacitance is substantially higher than that of the adhered membrane, the term C_{mem} may be neglected in the expression formulated in eq 3. In contrast, at high frequencies, the membrane capacitance, C_{mem}, and bulk membrane resistance, R_{mem}, dominate the impedance properties

(20) Bergveld, P.; van den Berg, A.; van der Wal, P. D.; Skowronska-Ptasinska, M.; Sudhölter, E. J. R.; Reinhoudt, D. N. *Sens. Actuators, B* **1989**, *18*, 309–327.

of the gate interface, and thus, the oxide layer capacitance, C_{ox}, can be neglected[18] (eq 4). The τ_2 value formulated in eq 4 is extracted from the intersect of the two linear segments of the transconductance curve at high frequencies (Figure 3). Knowing the values of τ_1 and τ_2, and knowing the capacitance of the oxide layer, C_{ox}, the respective R_{mem} and C_{mem} values are elucidated. The membrane capacitance is given by eq 5, where ϵ_o and ϵ_{mem}

$$C_{mem} = \epsilon_o \epsilon_{mem} A / \delta_{mem} \quad (5)$$

are the dielectric constant of the vacuum and of the membrane attached to the oxide layer, respectively ($\epsilon_o = 8.85 \times 10^{-12}$ F m^{1-}), A is the geometrical area of the layered membrane on the gate, and δ is the membrane thickness.

In the present study, we immobilize layered structures of antigen−antibody complexes on ISFET devices and apply impedance measurements to derive the transconductance curves of the respective systems. We use the experiments to characterize the thickness of the layers upon the buildup of the protein structures. The thickness values are used to characterize the surface coverage of the proteins on the gate. Furthermore, the impedance measurements are used to probe the sensing of antibodies or antigens by the functional gate interface. We compare the thickness values of the protein layers derived from the impedance studies with the thickness of related antigen−antibody structures elucidated by surface plasmon resonance measurements. We find that the impedance and SPR methods reveal comparable sensitivities. This suggests that the impedance measurements provide a powerful tool complementary to SPR to characterize layered protein structures on ISFET devices.

EXPERIMENTAL SECTION

Chemicals and Reagents. Avidin, biotin, *N*-2,4-dinitrophenyl-ϵ-amino-*n*-caproic acid (DNP-antigen), anti-*N*-2,4-dinitrophenyl-ϵ-amino-*n*-caproic acid from goat (anti-DNP-Ab), anti-goat IgG (whole molecule) biotin (anti-anti-DNP-Ab), protein G from *Streptococcus sp.*, cholera toxin (CT) from *Vibrio cholerae*, and *N*,*N*-di-(2,4-DNP)-L-cystine were purchased from Sigma, and biotinyl hexaethylene glycol dimer (dibiotin) was purchased from Pierce and used as supplied. Cystamine dihydrochloride was from Fluka, and glutaric dialdehyde (GDA; 50% w/w aqueous solution), (3-aminopropyl)triethoxysilane, and the other materials were purchased from Aldrich and used as supplied, without further purification. Monoclonal mouse IgG1-anti-B subunit of cholera toxin (CT-Ab) was purchased from Biodesign international (Kennebunk, ME). Ultrapure water from an Elgastat (UHQ) source was used throughout all the experiments. An aqueous solution of sodium chloride of low ionic strength, 0.01 M, was used as a background electrolyte solution in all the experiments.

Modification of the ISFET Devices. The primary modification of the Al_2O_3 gate of the ISFET was performed by positioning a 0.2-μL drop of (3-aminopropyl)triethoxysilane solution (10% v/v in toluene) that included 0.1 mL of water. Prior to the deposition of the mixture on the ISFET, the mixture was allowed to stand overnight to induce partial polymerization. The solution on the gate was further polymerized at 115 °C for 4 h in an oven (Eurotherm). The silylated chips were thoroughly rinsed with toluene followed by double-distilled water and dried in air at ambient temperature for 3 h. To prepare a sensor for anti-DNP-Ab sensing, the DNP-antigen was covalently linked to the silylated gate interface by the treatment of the chip in the DNP solution (2 mg mL^{-1}, 0.1 M HEPES, pH = 7.4) in the presence of EDC for 2 h, followed by rinsing with distilled H_2O. The resulting DNP-antigen-modified interface was reacted with various concentrations of the anti-DNP-Ab (in 0.1 M HEPES, pH = 7.4) for 30 min to yield the primary antigen−antibody complex. The resulting functionalized interface was then interacted with the biotin-conjugated anti-antibody (anti-goat IgG biotin) (10 mg mL^{-1} in PBS, pH = 7.4) for 30 min. Then the biotin-modified ISFETs were immersed in a solution of avidin (1 mg mL^{-1} in 0.1 M phosphate/saline buffer solution (PBS), pH = 7.4) for 30 min and thoroughly washed with the phosphate buffer. A second layer of avidin on the ISFET device was assembled by the interaction of the first avidin layer with a dibiotin solution (1 mg mL^{-1}, 0.1 M PBS, pH = 7.4) for 30 min followed by the reaction with avidin (1 mg mL^{-1}, 0.1 PBS, pH = 7.4, 30 min).

The ISFETs modified with protein G were prepared by treating the aminosiloxane-functionalized gate interface with glutaric dialdehyde solution (10% in 0.1 M PBS, pH = 7.4) for 20 min, followed by the reaction of the resulting interface with a solution of phosphate buffer (0.1 M, pH = 7.4) that included protein G (100 μg mL^{-1} in 0.1 M PBS, pH = 7.4) for 10 min. The resulting ISFETs were treated with the anti-cholera toxin antibody (anti-CT-Ab) (100 μg mL^{-1} in 0.1 M PBS, pH = 7.4) for 10 min to yield the sensing interface. The reaction between the Al_2O_3/aminosiloxane/GDA/protein G/anti-cholera toxin antibody sensing interface and the analyte cholera toxin was conducted by dipping the modified chip in PBS solution (0.1 M, pH = 7.4) that included various concentrations of cholera toxin for 20 min.

All the electrodes were subjected to the impedance analyses immediately after preparation.

Modification of the Gold Electrodes for SPR Measurements. Au-covered glass slides for SPR measurement were prepared by the same manner as Al_2O_3 ISFET devices with the exception that the gold plates were modified with *N*,*N*-di(2,4-DNP)-L-cystine, which allowed the direct functionalization of the electrodes with the DNP-antigen. To prepare the sensor for the SPR sensing of the cholera toxin, the Au-coated glass slides were first treated with cystamine dihydrochloride solution (20 mM in distilled H_2O) for 2 h. The resulting monolayer-functionalized surfaces were then modified with the protein G and the anti-CT-Ab by procedures similar to those described for the ISFET modifications.

Procedures for Impedance Measurements as ISFETs. The functionalized field-effect transistors (IMT, Neuchâtel, Switzerland), with an Al_2O_3 gate (20 × 700 μm^2) and a Pt wire (d = 0.8 mm) acting as a counter electrode and positioned 2 mm from the gate surface, were mounted in a cell filled with 0.8 mL of electrolyte solution. The ISFET characteristic curves (I_d against V_{ds} for the appropriate V_{gs} values) were recorded using an HP 4155 B semiconductor parameter analyzer.

The system described previously to carry out the impedance measurements on the ISFET devices[15] was upgraded by its computerized operation using LabView.

Dynamic impedance measurements were made using a Stanford Research lock-in amplifier model SR 830 DSP controlled by

LabView (National Instruments Co.). Figure 2 shows the scheme by which the ISFET is connected to the lock-in amplifier. The lock-in auxiliary outputs provide drain-source voltage, V_{DS}, gate-source bias, V_{GS}, and the operational amplifier power supply voltages. The reference signal (Sine Out) from the lock-in modulates the gate to give the ac signal V_{gs} through a 100-μF coupling capacitor, which also acts to remove dc back coupling to the lock-in amplifier. This ac modulation of the steady-state current, I_{DS}, becomes I_{gs}, which is converted to a voltage by the operational amplifier circuit, the output of which is connected to the A input port of the lock-in amplifier. The operational amplifier provides stable undistorted current-to-voltage conversion over a frequency range of 100 Hz to 100 kHz. A SKL MAS830L multimeter monitors the drain current, and a Tektronix model TDS 220 oscilloscope is used to monitor waveform shape.

In operating conditions, the drain-source current, I_{DS}, is set to 20 μA by first adjusting $V_{DS.}$ The value of the voltage depends on the particular ISFET being examined. Using a signal voltage, V_{gs}, further adjustment is made with V_{GS} at a value along with V_{DS}, so that no distortion is observed in the modulated wave and the I_{DS} value of 20 μA is kept. Modulating signals, V_{gs}, of the order of 50 mV were used. Using LabView control the gate voltage is swept by the lock-in from 100 Hz to 100 kHz. The resultant *in*-phase and quadrature components of the output are displayed by the lock-in amplifier and stored on a disk.

To determine the transconductance-transfer functions, the output potentials, V_{out}, at variable frequencies were related to the imaginary impedance, Z_{im}. The values of the output potentials, which correspond to Z_{im}, were normalized to the respective values at 100 Hz to give the respective transfer functions H_{im}. The imaginary impedance transfer function is given by eq 6. The errors

$$\log |H_{im}| = V_{out_{im}}(\text{f, Hz})/V_{out_{im}}(100\ \text{Hz}) \qquad (6)$$

in the calculated dimensions of the substrates were estimated to be ~10%.

Procedure for SPR Measurements. The SPR Kretschmann-type spectrometer (Biosuplar-2, Analytical-μSystem) (light-emitting diode light source $\lambda = 670$ nm) was used in this work. A high refraction index of the prism ($N = 1.61$) and a broad dynamic range (up to 19° in air) of the SPR instrument enabled SPR analyses of the modified surface without change in the initial angle. This is an important condition to provide correct computer fitting of the experimental data to a theoretical curve. The SPR data were processed using Biosuplar-2 software (version 2.2.30) on a PC computer. The experimental SPR spectra of the modified layers were fitted by theoretical curves by applying five-phase Fresnel calculation using the Nelder-Mead algorithm of minimization.[21]

The use of an open cell (230 μL) enabled easy elimination of the cell contents and thus rapid removal and change of solution, when necessary. Glass supports (TF-1 glass, 20 × 20 mm) covered with a chromium thin sublayer (~5 nm) and a polycrystalline gold layer (~50 nm) were supplied by Analytical-μ System and used for the SPR measurements.

(21) Beketov, G. V.; Shirshov, Y. M.; Shynkarenko, O. V.; Chegel, V. I. *Sens. Actuators, B* **1998**, *48*, 432−438.

RESULTS AND DISCUSSION

Scheme 1A depicts the configuration of the antigen−antibody model system for the analysis of anti-DNP-Ab by impedance measurements on the functionalized ISFET device. The Al_2O_3 gate interface of the ISFET is functionalized with an aminopropylsiloxane thin film. The antigen *N*-2,4-dinitrophenyl-ϵ-amino-*n*-caproic acid (**1**) was covalently linked to the modified gate. The resulting antigen interface is reacted with the anti-DNP-Ab to yield the primary antigen−antibody complex. The resulting functionalized interface is then interacted with the anti-anti-DNP-Ab and with avidin to yield the three-layer protein assembly. The subsequent reaction of the interface with the avidin generates an additional avidin layer on the surface. The specific architecture of the layered proteins on the gate interface of the ISFET device is designed in order to use the impedance technique as a tool to follow the buildup of the protein layers as a result of the primary antigen−antibody-anti-antibody complex formation on the gate surface. Furthermore, the secondary buildup of the avidin−dibiotin conjugate provides an amplification path for the primary generation of the antigen−antibody complex. At low coverage of the antigen−antibody complex, the impedance features of the gate might be only slightly perturbed, thus prohibiting sensitive detection of the immunological complex. The secondary buildup of the avidin−dibiotin layers would accumulate only if the initial antigen−antibody complex is generated on the gate surface. The perturbation of the impedance properties of the gate by the secondary protein layers would then amplify the initial formation of the antigen−antibody complex.

Figure 4 shows the transconductance curves at variable frequencies for the bare ISFET system, curve a, after the functionalization of the gate oxide surface with the aminopropylsiloxane film, curve b, its modification with the dinitrophenyl antigen, (**1**), curve c, and after the stepwise assembly of the protein layers according to Scheme 1A, curves d−g. In this experiment, the antigen-functionalized gate is interacted with a high concentration of the anti-DNP-Ab, 10 μg mL^{-1}. This results in an almost saturated layer of the antigen−anti-DNP-Ab complex on the gate surface. From the transconductance curve that corresponds to the aminosiloxane-functionalized layer, and its dielectric constant, we calculate the film thickness to be 245 ± 20 Å. Since the dielectric constants of the aminopropylsiloxane film and the protein layers are almost identical (refractive indexes for the aminosiloxane and protein correspond to $n = 1.43$ and 1.45, respectively), we may assume a constant dielectric constant of the functional membrane upon its buildup on the ISFET oxide interface. The covalent binding of the dinitrophenyl antigen to the aminosiloxane membrane does not change the transconductance curve of the functional membrane since its thickness is too low to observe capacitance/resistance changes of the membrane. Curves d and e of Figure 4 show the transconductance curves observed upon the association of the anti-DNP-Ab to antigen-functionalized membrane and of the biotinylated anti-Fc-antibody that links to the anti-DNP-Ab, respectively. The τ_2 values alter from 15.7 to 19.0 and 22.4 μs, respectively, while the τ_1 values are almost unaltered, 1.26 ± 0.02 ms. Thus, the association of the anti-DNP-Ab and the anti-antibody to the functional interface mainly alters the capacitance of the membrane. Using eqs 3−5, we estimate the thickness of the anti-DNP-Ab layer to be ~87 ±

Scheme 1. Stepwise Assembly of the Sensing Interface (A) for the Amplified Impedance Analysis of Anti-dinitrophenyl Antibody on the ISFET Devices and (B) for Analyzing the Anti-dinitrophenyl Antibody Using SPR Spectroscopy

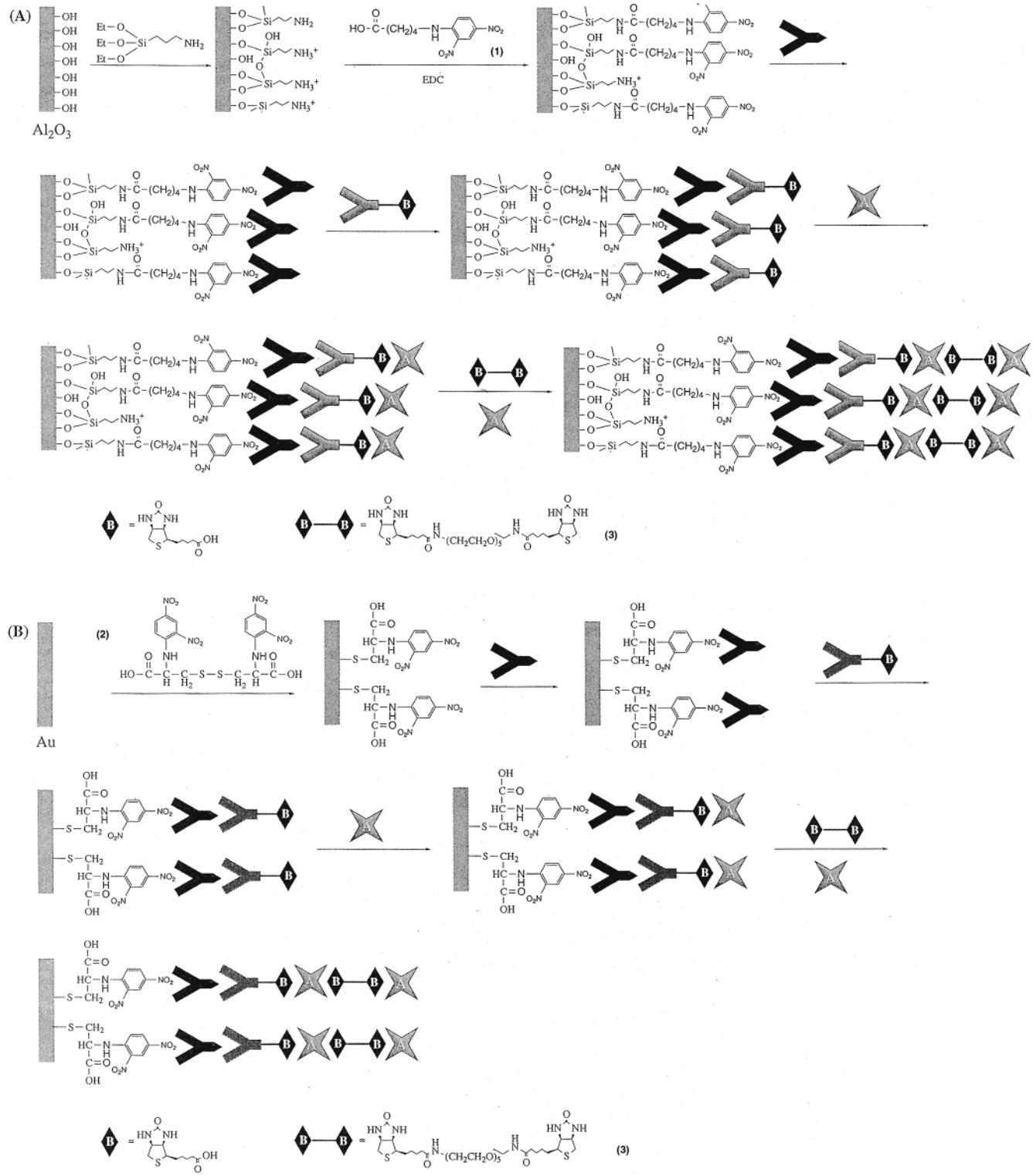

8 Å, and the thickness of the protein layer increases by 42 ± 4 Å as a result of the association of the biotinylated anti-anti-DNP-Ab. It should be noted that the aminosiloxane film represents a porosive rough membrane. The anti-DNP-Ab may bind to inner membrane pores that do not add to the geometrical thickness value of the protein layer. The anti-DNP-Ab exhibits a nonsymmetrical geometry with dimensions of ~50 × 70 × 100 Å that translates to a surface coverage of the anti-DNP-Ab of ~4.1 × 10^{-12} mol cm^{-2}. The increase in the thickness of the protein layers upon the binding of the biotinylated anti-Fc-antibody is only ~20% of the coverage of the anti-DNP-Ab (the anti-DNP-Ab and anti-anti-DNP-Ab exhibit similar dimensions), which corresponds to a surface coverage of the anti-anti-DNP-Ab of ~8.2 × 10^{-13} mol cm^{-2}. This may be attributed to two reasons: (i) Each anti-Fc-

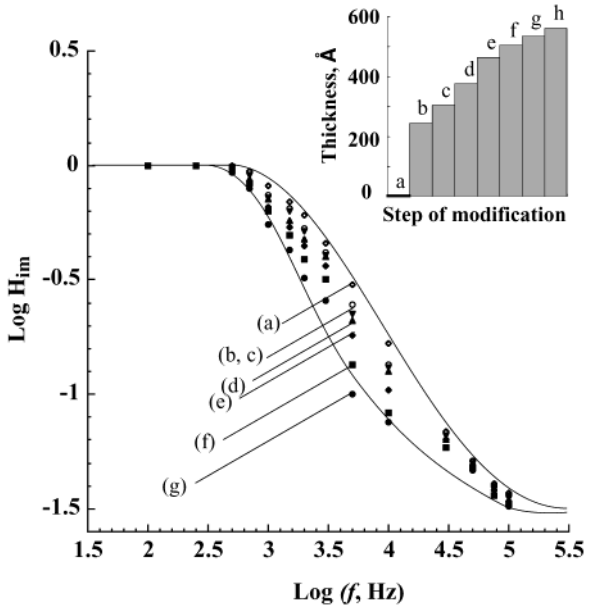

Figure 4. Transconductance, H_{im}, curves at the following variable frequencies: (a) bare ISFET device, (b) aminopropylsiloxane-functionalized ISFET, (c) after modification of the gate oxide interface with the dinitrophenyl-antigen, (d) after the assembly of the anti-dinitrophenyl antibody (10 μg mL^{-1}), (e) after immobilization of the anti-anti-dinitrophenyl antibody, (f) and (g) after coupling of the sensing interface with one and two avidin layers, respectively. Inset shows stepwise thickness changes of the membrane upon the buildup of the layered assembly on the ISFET gate interface: (a) and (b) correspond to the bare ISFET and aminosiloxane-functionalized gate interface, respectively; (c), (d), and (e) correspond to binding of 0.1, 1.0, and 10.0 μg mL^{-1} anti-DNP-Ab, respectively; (f) corresponds to the binding of the biotinylated anti-anti-DNP-Ab; (g) and (h) correspond to the association of the first and second layers of avidin to the interface, respectively.

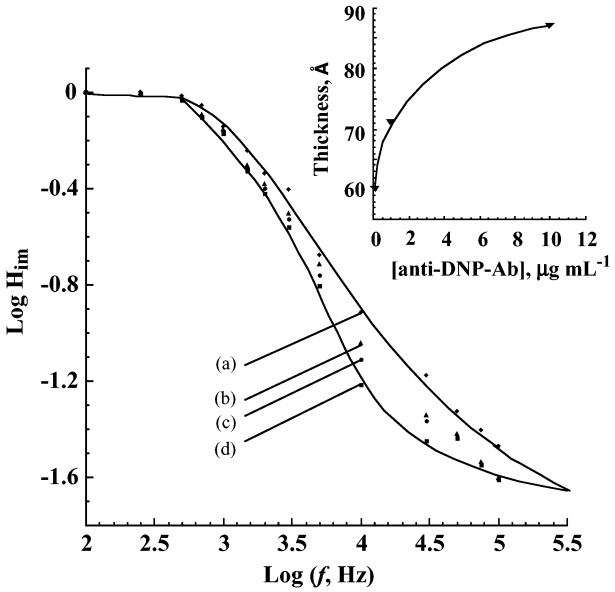

Figure 5. Transconductance, H_{im}, curves at variable frequencies corresponding to the following: (a) the DNP-antigen-functionalized ISFET device, and after the interaction of the sensing device with (b) 0.1, (c) 1.0, and (d) 10.0 μg mL^{-1} of the anti-DNP-Ab. Inset: stepwise change of the membrane thickness upon the treatment of the DNP-antigen-functionalized ISFET device with various concentrations of the anti-DNP-Ab.

antibody includes two binding sites for the Fc-fragment of the anti-DNP-Ab, and hence, the theoretical surface coverage of the anti-anti-DNP-Ab should be 50% of a saturated layer of the anti-DNP-Ab. (ii) The aminopropylsiloxane film functionalized with the antigen−antibody complex represents a rough interface. Thus, the binding of the anti-anti-DNP-Ab to the rough surface might be sterically prohibited. Curves f and g of Figure 4 show the transconductance curves of the functionalized membrane after the binding of the first layer of avidin and after the association of the second avidin layer with the dibiotin cross-linking units. As before, the association of the avidin layers induces changes mainly in the τ_2 values to 32.3 and 47.8 μs, implying that the association of the proteins results in the alteration of the membrane capacitance. Using eqs 3−5, the changes in the transconductance curves upon the binding of avidin translate to a thickness of 30 ± 3 Å of the first avidin layer and an additional increase in the membrane thickness of 31 ± 3 Å as a result of the association of the second avidin layer. The diameter of avidin is 62 ± 4 Å (Protein Data Bank, Brookhaven National Laboratory[22]). Thus, the surface coverage of the membrane by an avidin layer is ~3.5×10^{-12} mol cm^{-2}. This loading appears to be slightly overestimated. This may be attributed to the contribution from the dibiotin cross-linking units to the film thickness and to the eventual contribution of the protein dielectric constant to the dielectric constant at the resulting membrane. Note that an increase in the membrane permeability would result in a higher value of the membrane thickness. The Figure 4 inset shows the gradual thickness change of the membrane upon the buildup of the layers according to Scheme 1A.

Control experiments reveal that the changes in the transconductance curves originate from the specific biorecognition events occurring on the antigen-functionalized interface. Exclusion of the anti-DNP-Ab or the biotinylated anti-anti-DNP-Ab from the systems prevents the association of the subsequent biomaterials to the membrane interface, and no changes in the transconductance curves are observed. This implies that nonspecific adsorption of the biocomponents to the membrane interface are insignificant to change the impedance features of the gate. Thus, the observed changes in the transconductance curves originate from specific biorecognition events in the layered protein constructions. Indeed, the impedance changes of the ISFET membrane as a result of the association of the anti-DNP-Ab may be used to sense the antibody. Figure 5 shows the transconductance curves recorded upon the treatment of the DNP-antigen-functionalized membrane with various concentrations of the anti-DNP-Ab. It can be seen that as the concentration of anti-DNP-Ab is elevated, enhanced changes in the τ_2 values (membrane capacitances) are observed. These values result in the membrane thickness variations depicted in the Figure 5 inset.

The analogous analysis of the anti-DNP-Ab and the subsequent association of the biotinylated anti-Fc-antibody and the avidin-dibiotin layers was conducted using SPR as the read-out signal. In this experiment, a gold-covered glass support acts as the transducer. The *N*,*N*-di(2,4-DNP)-L-cystine (**2**), was covalently coupled to the gold surface via S-functionalities. Figure 6 shows the SPR spectra of the antigen-functionalized electrode before the

(22) http:// www.rcsb.org/pdb.

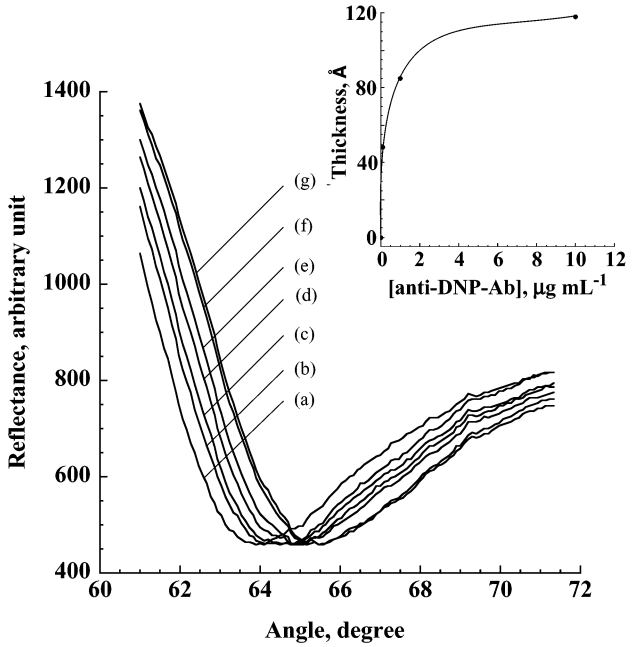

Figure 6. SPR spectra of the following: (a) the DNP-antigen-functionalized Au-surface, and upon its treatment with (b) 0.1, (c) 1.0, and (d) 10.0 μg mL^{-1} anti-DNP-Ab; (e) upon the assembly of the biotinylated anti-anti-DNP-Ab layer, and (f) and (g) after the association of one and two layers of avidin, respectively. Inset: stepwise thickness changes of the membrane upon the buildup of the layered assembly on the glass Au-coated SPR plate.

interaction with the anti-DNP-Ab, curve a, and those obtained upon treatment of the surface with various concentrations of the anti-DNP-Ab, curves b−d; cf. Scheme 1B. Clearly, as the bulk concentration of the anti-DNP-Ab increases, the minimum reflectivity angle is shifted to higher values. Theoretical fitting of the experimental SPR spectra revealed film thicknesses of the anti-DNP-Ab monolayer that correspond to 48 ± 3, 82 ± 6, and 116 ± 8 Å at bulk concentrations of the anti-DNP-Ab of 0.1, 1.0, and 10.0 μg mL^{-1}, respectively. In SPR spectroscopy, adsorbed layers are largely characterized in terms of effective thickness, δ, and effective refraction index, n_e. In the case of densely packed monolayers, this assumption is correct for ordered biomolecular adsorption. In this work, we apply an additional approach considered in detail elsewhere[23,24] to characterize protein layers using SPR. In accordance with this approach, the protein surface coverage, N_s, and its polarizability, A_m, are determined instead of its effective thickness and the refractive index.

For an isotropic layer of protein molecules, an expression for a reflection coefficient is defined by eq 7,[24] where R_p is the integral

$$R_p = \overline{R_{0p}} + 2\pi i N_s A_m[(\beta g_{xx} - f_{zz})(1 + \overline{R_{0p}}^2) - 2(\beta g_{xx} + f_{zz})\overline{R_{0p}}]/[(1 + 2\pi i N_s A_m)(\beta + 2\pi i N_s A_m f_{zz}) - 2\pi i N_s A_m(\beta g_{xx} - f_{zz})\overline{R_{0p}}] \quad (7)$$

Fresnel's reflection coefficient of the system for p-polarization,

(23) Baryakhtar, I. V.; Demidenko, Y. V.; Kriuchenko, S. V.; Lozovskii, V. Z. *Surf. Sci.* **1995**, 323, 142−150.

(24) Shirshov, Y. M.; Chegel, V. I.; Subbota, Y. V.; Matsas, E. P.; Rachcov, A. E.; Sergeeva, T. A. *SPIE Proc.* **1995**, 2648, 118−123.

Table 1. Comparison of the Thicknesses of the Membrane Layers upon Sensing of the Anti-DNP Antibody Using Impedance Measurements on ISFET Devices and SPR Analyses

	estimated thickness, nm	
modified surface	ISFET	SPR
aminosiloxane	24.5	
anti-DNP-Ab (μg mL^{-1})		
0.1	6.0	4.8
1.0	7.1	8.2
10.0	8.7	11.6
anti-anti-DNP-Ab	4.2	3.7
avidin1	3.0	4.4
avidin 2	3.1	1.5

$\overline{R_{0p}}$ is the integral Fresnel's reflection coefficient of the system for p-polarization in the absence of the adsorbed molecular layer, β is a constant expressed as $\beta = 1 + 4\pi A_m/n_m^2$, where n_m is the refractive index of the bulk medium, and g_{xx} and f_{zz} are combinations of the wave vectors.[23] The molecule polarizability, A_m, can be expressed in the form of eq 8, where n_p is the refractive index

$$A_m = 3M(n_p^2 - 1)/4\pi\rho N_a(n_p^2 + 2) \quad (8)$$

of condensed proteins, M is the molecular weight of the protein, ρ is the protein density, and N_a represents the Avogadro number.

The value of a surface coverage of a biomolecular monolayer can be calculated using eqs 7 and 8, since the refractive indexes of proteins vary in a narrow range ($n_p = 1.42-1.48$), and thus the protein refractive index can be considered to be constant and it corresponds to $n_p = 1.45$. In our case, this approach resulted in a surface coverage of the anti-DNP-Ab (10.0 μg mL^{-1}) of 4.15 × 10^{-12} mol cm^{-2} that agrees perfectly with that estimated using impedance ISFET measurements.

Table 1 compares the thicknesses of the anti-DNP-Ab interface observed upon the treatment of the antigen-functionalized Al_2O_3 gate or the Au-covered plate surfaces. Even though the base antigen interface configurations in the siloxane thin-film assembly or thiolated monolayer differ in the two systems, comparable thickness values of the associated anti-DNP-Ab layers are detected by the two methods. Figure 6, curve e, shows the SPR spectrum obtained after treatment of the antigen−DNP-Ab complex layer (generated at a concentration of 10.0 μg mL^{-1} anti-DNP-Ab) with the biotinylated anti-Fc-Ab. Theoretical fitting of the spectrum indicates that the associated anti-anti-DNP-Ab film thickness is 37 ± 3 Å, a value that is very similar to that observed for the analogous step in the functional ISFET device (42 ± 4 Å). Curves f and g of Figure 6 show the SPR spectra of the system after the stepwise assembly of the avidin layers using the dibiotin (**3**) cross-linker on the antibody/anti-antibody interface. The theoretical fitting of these curves indicates that the thicknesses of the first and second avidin layers corresponds to 44 ± 3 and 15 ± 1 Å, respectively. The Figure 6 inset outlines the gradual change of the membrane thickness upon the buildup of the layers according to Scheme 1B.

The impedance analysis of antigen−antibody interactions using the ISFET transducer was applied to develop a sensing device for the cholera toxin. For this system too, the impedance

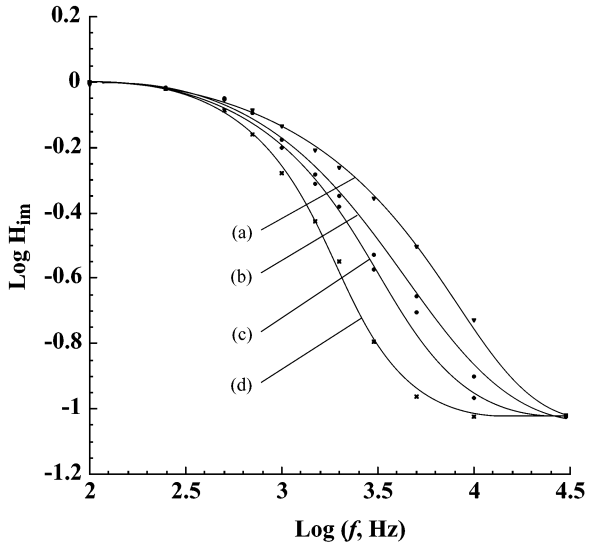

Figure 7. Transconductance, H_{im}, curves at the following variable frequencies: (a) bare ISFET device; (b) protein G-modified ISFET device; (c) after assembly of the anti-cholera toxin−antibody layer, and (d) after binding of the cholera toxin−antigen layer (1.0×10^{-7} M).

measurements on the ISFET device were accompanied by SPR analyses of the cholera toxin, using the analogous sensing configuration. Scheme 2A outlines the detection path of the cholera toxin on the ISFET devices. The oxide layer of the gate is modified with an aminopropylsiloxane film. Protein G is covalently linked to the surface using glutaric dialdehyde as a coupling reagent, and the anti-cholera toxin antibody (anti-CT-Ab) is associated with the protein G interface and acts as the sensing interface. The binding of the CT to the antibody is anticipated to alter the impedance features of the gate interface. Figure 7 shows the transconductance curves that result upon buildup of the protein G interface, curve b, the association of the anti-CT-Ab, curve c, and the binding of the CT-antigen to the sensing interface, curve d. The CT that is sensed by the functional ISFET device exhibits a high bulk concentration, 10^{-7} M. The transconductance curves reveal that the buildup of the protein layers results in significant changes in the τ_2 values from 79.4 μs for the bare chip to 0.24 ms for the chip modified with 10^{-7} M CT, while the τ_1 values are almost unchanged, $\sim$1.26 $\pm$ 0.02 ms. Thus, the assembly of the protein layers on the ISFET results mainly in capacitance changes of the membrane. Using eqs 3−5, we can estimate the thickness changes of the membrane as a result of the buildup of the protein layers (Table 2). We find that the protein G interface exhibits a thickness of 22 $\pm$ 2 Å that translates to a surface coverage of $\sim 6.5 \times 10^{-13}$ mol cm^{-2}. Due to the rough interface of the aminosiloxane film, it is expected that protein G binds to microscopic porous domains, and thus, its real surface coverage is not fully reflected in the calculated thickness parameter. The association of the anti-CT-Ab to protein G yields a further increase in the membrane thickness that corresponds to 36 $\pm$ 4 Å or a surface coverage of $\sim 1.2 \times 10^{-12}$ mol cm^{-2}. Upon analyzing the CT, the thickness of the sensing membrane increases by 152 $\pm$ 15 Å at the CT concentration of 10^{-7} M. From the respective size of the CT-antigen, we estimate its surface coverage to be $\sim 1.2 \times 10^{-12}$ mol cm^{-2}, which is in good agreement with the estimated surface coverage of the anti-CT-Ab.

Table 2. Comparison of Thicknesses of the Membrane Layers upon the Analysis of Cholera Toxin by ISFET Devices and SPR Measurements

	estimated thickness, nm	
modified surface	ISFET	SPR
aminosiloxane	29.8	
protein G	2.2	5.6
Ab-cholera toxin	3.6	3.0
cholera toxin (M)		
10^{-11}	5.9	3.9
10^{-9}	9.7	9.6
10^{-7}	15.2	11.4

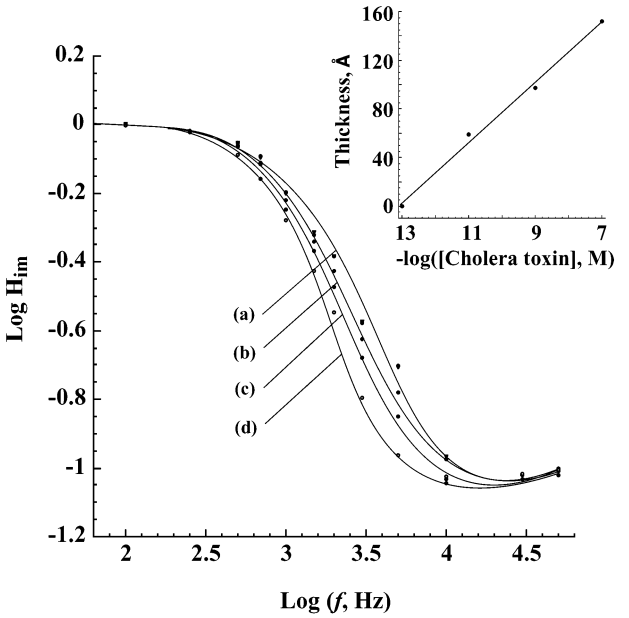

Figure 8. Transconductance, H_{im}, curves of the following: (a) anti-cholera toxin antibody-functionalized ISFET device upon sensing of (b) 1.0×10^{-11}, (c) 1.0×10^{-9}, and (d) 1.0×10^{-7} M cholera toxin antigen. Inset: stepwise change in the membrane thickness upon the treatment of the anti-cholera toxin-antibody-functionalized ISFET device with various concentrations of the cholera toxin−antigen.

Figure 8 shows the transconductance curves corresponding to the analysis of different concentrations of the CT-antigen by the antibody-functionalized ISFET gate. As the concentration of the CT is elevated, the transconductance curves are shifted to lower τ_2 values, while the τ_1 values are almost unaltered. It is evident that a CT concentration corresponding to 10^{-11} M can be sensed by the method, and this value may be considered as the lower detection limit. The lethal concentration[25] of CT is 0.1 μg mL^{-1}, and thus, we are able to detect the toxin at levels that are $\sim 10^4$ lower than the lethal value. From the respective transconductance curves, the thickness of the CT-antigen linked to the antibody is calculated. As the bulk concentration of CT increases, the content of the surface-associated toxin is higher (see inset in Figure 8). Knowing the dimensions of the CT, and approximating a footprint of $\sim 1 \times 10^{-16}$ Å^2, we estimate the surface coverage of

(25) Jawetz, E.; Melnick, J. L.; Adelberg, E. A. *Review of Medical Microbiology*, 15th ed.; Lange Medical Publications: Los Altos, CA, 1982; Chapter 18, p 227.

Scheme 2. Assembly of the Sensing Interface and the Detection Path for Analyzing Cholera Toxin (A) By Means of Impedance Measurements on ISFET Devices and (B) By Means of SPR Spectroscopy

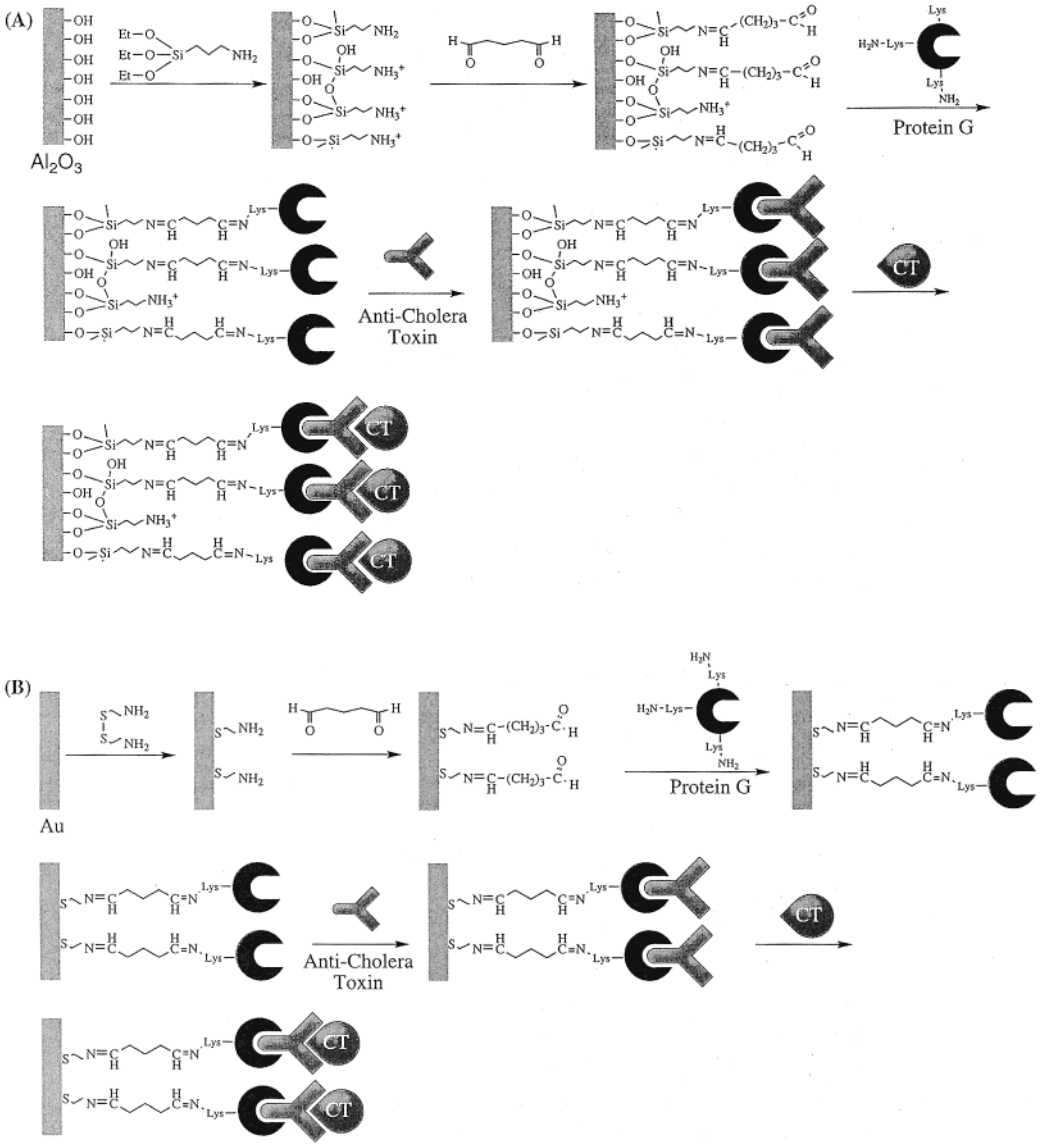

the toxin to be 4.6×10^{-13}, 7.6×10^{-13}, and 1.2×10^{-12} mol cm^{-2}, at bulk concentrations of 1.0×10^{-11}, 1.0×10^{-9}, and 1.0×10^{-7} M, respectively.

Scheme 2B shows an analogous configuration for the analysis of the CT on an Au surface by SPR. The protein G is covalently linked to a cystamine monolayer, and anti-CT-Ab is further linked to the protein G layer to yield the sensing interface. Figure 9 shows the SPR spectra of the cystamine monolayer-modified Au-surface, curve a, after the covalent linkage of the protein G to the monolayer, curve b, and after the association of the anti-CT-Ab, curve c. The minimum reflectivity angle is shifted to higher angles as the layers of protein G and the anti-CT-Ab are linked to the surface. Theoretical fitting of the experimental SPR spectra shown in curves b and c indicates that the thickness of the protein G layer and the anti-CT-Ab layer are 56 ± 4 and 30 ± 2 Å, respectively. Interestingly, the thickness of the anti-CT-Ab layer on the Au surface is comparable to the thickness of the analogous layer on the ISFET membrane. On the other hand, the thickness of the protein G layer on the gold support is substantially higher than the thickness of the respective layer on the ISFET (Table 2). This is probably due to the fact that the protein G binds to a relatively smooth Au surface, whereas the binding of the protein G to the oxide layer of the ISFET occurs on a rough porous surface. The binding of the protein G in pores of the oxide interface is not reflected in the resulting thickness values. The secondary binding of the anti-CT-Ab to the protein G units linked to the membrane surface and pores leads to the protein units that are exposed on the surface of the ISFET membrane. As a result, the thickness of the anti-CT-Ab layer on the ISFET is very similar to the thickness of the analogous antibody layer on the smooth gold support. Treatment of the antibody-functionalized surface with various concentrations of the CT results in the SPR spectra shown in curves d−f. As the bulk concentration of the CT increases, the minimum reflectivity angle is shifted to higher values. By fitting

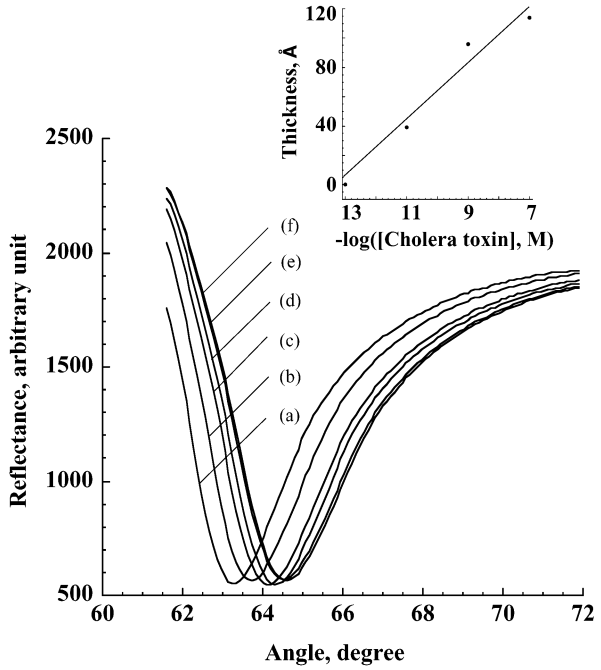

Figure 9. SPR spectra of the following: (a) cystamine-modified Au-coated glass surface; (b) after the immobilization of protein G; (c) after the association of the anti-cholera toxin antibody, upon treatment of the anti-cholera toxin antibody-functionalized Au-coated glass electrode with (d) 1.0×10^{-11}, (e) 1.0×10^{-9}, and (f) 1.0×10^{-7} M of the cholera toxin-antigen. Inset: stepwise change in the membrane thickness upon the treatment of the anti-cholera toxin-antibody-functionalized Au-coated glass electrode with various concentrations of the cholera toxin-antigen.

the experimental curves, the thicknesses of the CT layers are 39 $\pm$ 2, 96 $\pm$ 7, and 114 $\pm$ 8 Å for bulk concentrations corresponding to 1.0×10^{-11}, 1.0×10^{-9}, and 1.0×10^{-7} M, respectively. We see that although the base layer of the protein G membrane on the ISFET differs substantially from the protein G interface generated on the cystamine monolayer, the surface-linked anti-CT-Ab sensing layer reveals comparable surface coverage in the two systems. Also, the thicknesses of the CT layers formed on the sensing antibody interfaces reveal comparable magnitudes upon the application of the SPR and impedance methods. The same also is true for a surface coverage of the cholera toxin antigen adsorbed on the anti-CT-Ab-functionalized surfaces of the ISFET devices and SPR electrodes (4.6×10^{-13}, 7.6×10^{-13}, and 1.2×10^{-12} mol cm^{-2} obtained using impedance measurements on the ISFET devices and 5.1×10^{-13}, 8.6×10^{-13}, and 1.4×10^{-12} mol cm^{-2} obtained using SPR measurements at the bulk concentrations of CT of 1.0×10^{-11}, 1.0×10^{-9}, and 1.0×10^{-7} M, respectively).

CONCLUSIONS

The present study has demonstrated the application of impedance measurements on the ISFET devices as a means of analyzing antigen−antibody interactions. The analysis of the impedance features of the sensing interface enabled us to identify the composition and structure of the antigen−antibody layers on the gate surface. We have performed complementary SPR measurements on analogous systems that were studied by impedance measurements on the ISFET devices. Our study implies that the two methods yield very similar information. Surface plasmon resonance is already a well-established technique for the probing of protein−protein or antigen−antibody recognition processes, and various biosensors are based on this method. We suggest that impedance measurements on an ISFET device could be an alternative route to develop biosensors and for probing biorecognition events. For this purpose, one does not need to record the transconductance curve in a broad region of frequencies, but to record the transconductance at a specific frequency. Thus, besides the fundamental information that can be extracted from the impedance measurements on the structure of proteins on the surface, the method may be considered as a general transduction means of biosensing processes.

ACKNOWLEDGMENT

This research is supported by the Max Planck Award for International Cooperation (Germany). The authors thank Mr. Julian Wasserman for his assistance in the construction of the setup for performing the impedance measurements on ISFETs.

Received for review May 8, 2002. Accepted June 26, 2002.

AC020312F